Journal of Magnetism and Magnetic Materials 557 (2022) 169461

Contents lists available at ScienceDirect

Journal of Magnetism and Magnetic Materials

journal homepage: www.elsevier.com/locate/jmmm

Tuning the magnetic properties of Fe thin films with RF-sputtered amorphous carbon

Shoug Alghamdi [a,b], Timothy Moorsom [a], Fatma Al Ma'Mari [a,c], Alistair Walton [a], Zabeada Aslam [d], Mannan Ali [a], Bryan J. Hickey [a], Oscar Cespedes [a,*]

[a] School of Physics and Astronomy, University of Leeds, LS2 9JT Leeds, UK
[b] Department of Physics, Faculty of Science, Taibah University, Yanbu 46423, Saudi Arabia
[c] Department of Physics, Sultan Qaboos University, 123 Muscat, Oman
[d] School of Chemical and Process Engineering, University of Leeds, LS2 9JT Leeds, UK

ARTICLE INFO

Keywords:
Molecular spintronics
Magnetism
Amorphous carbon

ABSTRACT

RF-sputtered amorphous carbon (a-C) offers a simple and cheap pathway to tune the magnetic properties of transition metal thin films for magnetic memories and different spintronic applications. This paper describes changes in the magnetic properties of iron thin films with a-C overlayers. In as-deposited samples, hybridisation and intermixing at the Fe/a-C interface leads to magnetic softening (Liu et al., 2006) [1], with a reduction in the coercive field (H_c) up to a factor of five for Fe/a-C/Fe trilayers, and a 10–30% lower saturation magnetization as a function of the metal film thickness. After annealing at 500 °C, inter-diffusion and graphitization of the carbon layer results in up to a factor five increased coercivity due to increased pinning as shown via Kerr microscopy. Therefore, RF-sputtered carbon overlayers and post-processing can tune the anisotropy and domain configuration of metallic thin films in a synthesis methodology that is simple, cheap and sustainable.

1. Introduction

Magnets are required in many everyday applications from sensing to energy generation and information storage. [2,3] Heavy metals are frequently combined with transition metal ferromagnets to produce compounds or multilayers with the desired magnetic properties for each application. [4] For example, compounds of FM material with rare earth elements, such as neodymium iron boron (NdFeB) and samarium cobalt (Sm-Co) leads to increase the magnetic energy product $(BH)_{max}$ up to 290 kJ/m [3]. [3–5] At the same time, noble metals such as Pt or Ir are used to change the magnetic anisotropy and interface interactions in thin films for magnetic storage applications. [6,7] In order to become sustainable for the long-term future, these heavy and rare metals will need to be replaced with eco-friendly alternatives of similar performance. Polycrystalline sputtered iron and carbon, because of their abundance and easy, eco-friendly processing, represent probably the cheapest and most sustainable combination of elements for thin film magnetism. The magnetic properties of nanocomposites, thin films and hybrid iron-carbon compounds have been studied extensively, although a systematic approach to thin film tunability in thickness, layer structure and post-processing is lacking. [8–12]

Large changes in the anisotropy and magnetization of cobalt and iron can be obtained by using nanocarbon materials such as C_{60}, [13–16] and it has been shown that spin ordering can be induced in non-magnetic metals by this molecule. [17–19] Measurements in carbon nanotubes gave evidence for contact-induced magnetism at the interface with a ferromagnet, [20] and interactions with magnetic nanocomposites. [21] The coupling between ferromagnet and carbon-based molecules can extend through normal metal layers of nm thickness. [22] A Ni/graphene interface has also studied and the results show a strong hybridisation effect between the graphene π and 3d bands in Ni. [23] Spin-polarised charge transfer and hybridisation between the π -carbon orbitals and the d-orbitals of transition metals lead to the formation of hybrid metal-carbon states, so the magnetic properties can be altered due to spin-polarised charge transfer. Molecular materials can also lead to a shift in the hysteresis loop that has been identified as exchange bias, although its origin could be connected to molecular dynamics and the formation of spin polarised electrical dipoles. [16,24] Changes observed underline the importance of hybridisation and electron transfer as a means to tune interfaces of itinerant ferromagnets using nanocarbon materials. They also put in relevance the potential role of amorphous carbon layers in heat-assisted magnetic recording (HMAR). [25]

* Corresponding author.

https://doi.org/10.1016/j.jmmm.2022.169461
Received 12 January 2022; Received in revised form 28 April 2022; Accepted 5 May 2022
Available online 11 May 2022

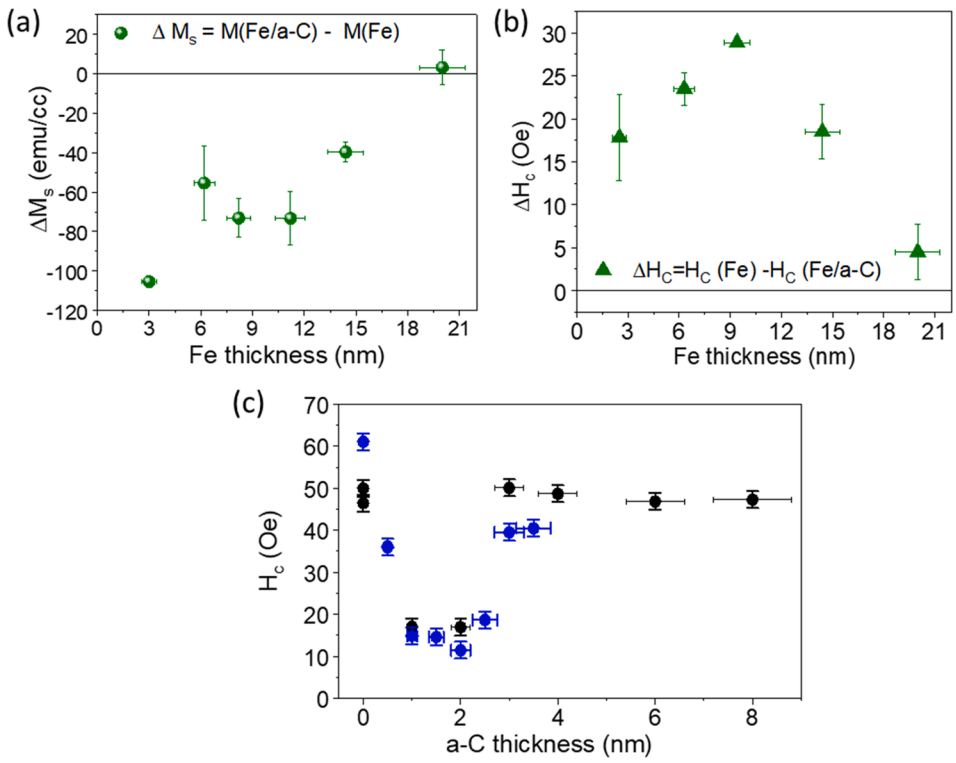

Fig. 1. Magnetic measurements of as-grown samples. (a) Change in room temperature Ms for Ta(3)/Fe(t)/a-C(5)/Al(5) compared with control samples of Ta(3)/Fe (t)/Al(5), where (t) is the varying Fe thickness. (b) The difference in the coercivity, H_c, between Fe and Fe/a-C as a function of Fe thickness. Results in (a) and (b) are averaged over 10 samples for each data point. (c) H_c vs a-C layer thickness (t) in Ta(3)/Fe(10)/a-C(t)/Fe(10)/Ta(5) trilayers. All thicknesses given in nm.

In this paper, we focus on RF-sputtered amorphous carbon (a-C). This material has ideal qualities for thin film technologies, including compatibility with UHV and lithographic processes, very low price for the target material, low thin film roughness (~Å) when deposited at room temperature and chemical stability at a wide range of temperature and conditions. Amorphous carbon is used for example as coating in hard disks. [26,27] Furthermore, amorphous carbon thin films display outstanding mechanical, chemical, and optical features, accredited to the flexibility of *sp* hybridisation. [28,29] There have been previous studies on the mechanical and magnetic properties of metal/a-C compounds. Coupling metal films with carbon layers can enhance the graphitisation of carbon when a-C films are heated between 425 °C and 600 °C for minutes to hours. [29–31] Transmission electron microscopy (TEM) confirmed carbon diffusion and crystallisation of a-C/Co/a-C trilayers when annealed between 500 °C and 600 °C. [32,33] Annealing between 400 °C and 600 °C for 2 h can increase the coercivity (H_c) of carbon /cobalt chromium platinum alloys (CoCrPt) from 510 Oe to 650 Oe. The formation of a continuous layer of cementite (Fe_3C, an iron carbide phase) leads to a higher saturation magnetization. [34–38] However, as the annealing temperature is increased to 550 °C, a-C atoms diffuse into the Fe layer, and eventually create a nano-graphitic phase. [39,40] Here, we show that it is possible to tune the anisotropy of iron thin films using a-C interfaces, increasing or decreasing the coercivity depending on the sample structure and post-deposition annealing.

2. Results

2.1. Magnetometry in as-grown bilayers and trilayers

Our Fe/a-C bilayer samples have the structure Si(substrate)//Ta(3 nm)/Fe(t)/a-C(5 nm)/Al(5 nm), where (t) ranged from 3 nm to 20 nm. Control samples with an a-C layer were also grown for comparison. The magnetic in-plane easy axis is determined by a forming field of 300 Oe during sputtering. We carry out all our magnetic measurements along this in-plane axis. We observe a reduction in M_s when the a-C layer is included in the structure. This change is roughly equivalent to one iron atom layer (Fig. 1 a), and we attribute it to the formation of a low magnetization Fe/a-C interface. We also measure a reduction in the coercive field (H_c) of Fe thin films with a-C layers, Fig. 1 b. Bulk properties dominate when the Fe thickness is $\geq$ 20 nm, with nil or small changes to magnetization and coercivity above that thickness. The inverse dependence with the thickness of the ferromagnet puts in relevance the interfacial characteristic of the effect.

In order to study the magnetic coupling *across* the carbon layer, we grow trilayer Fe/a-C/Fe samples with the structure: Ta(3 nm)/Fe(10 nm)/a-C(t)/Fe(10 nm)/Ta(5 nm), with t = 0–8 nm. Samples with a-C thicknesses of 1 and 2 nm show a large reduction in coercivity of up to a factor 5–6. Interestingly, this demonstrates a magnetic coupling of Fe films across thin a-C layers, leading to a larger magnetic softening. This coupling between interfaces requires a continuous carbon layer, so the effect is reduced when t(a-C) $\lesssim$ 1 nm. However, as the a-C layer becomes thicker than 2–3 nm, the coupling also becomes smaller, increasing H_c to the values of Fe control films without a-C. We think that this reduction in the coercivity and interlayer coupling is due to a small, induced magnetization of the a-C layer via spin polarized charge transfer and orbital re-hybridisation, as it is the case in other nanocarbon layers. Once the separation between the Fe layers exceeds the propagation of this proximity effect, the trilayers de-couple and recover the coercivity found in the control samples.

2.2. Magnetometry in annealed bilayers and trilayers

There is an increase in M_s when Fe/a-C bilayer samples are annealed up to 200 °C in vacuum (10^{-5} Torr) for one hour. This may be evidence of improved crystallinity in the Fe/RF- sputtered a-C structure. M_s values in Al capped samples above those of pure Fe are probably due to the formation of Fe_3C. However, the magnetization drops with annealing temperatures above 400 °C for samples capped with Al or Nb, as

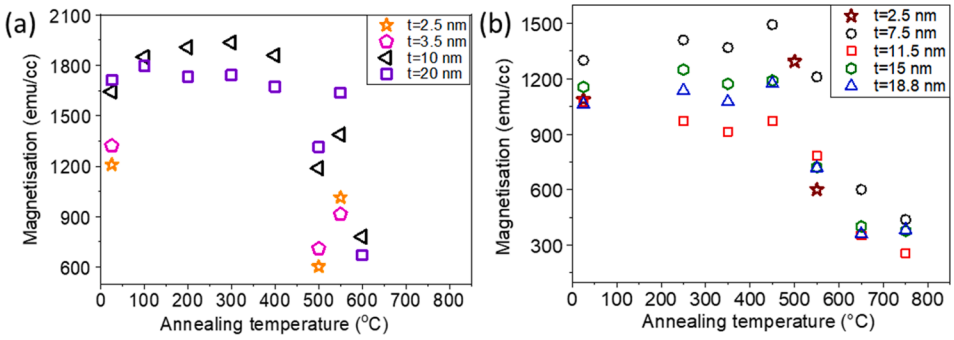

Fig. 2. Magnetization for Ta(3 nm)/Fe(t)/a-C (5 nm)/cap(5 nm) samples, with t = 2.5–20 nm and Al (a) or Nb (b) cap. Samples annealed for one hour in vacuum. The first data points at 25 °C represent the samples before annealing.

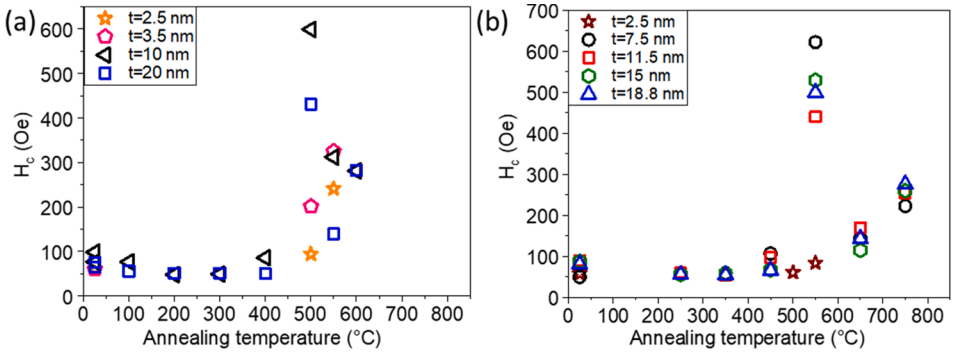

Fig. 3. Effect of annealing temperatures on coercivity using different capping layers (a) 5 nm of Al (b) 5 nm of Nb. All of the samples were grown on top of Fe/RF-sputtered a-C with the structure and Si/SiO_2//Ta(3 nm)/Fe(t)/a-C(5 nm)/cap (Al (5 nm)) or (Nb (5 nm)), where 2 nm < (t) < 20 nm. The H_c values were extracted from in-plane M-H loops measured at room temperature.

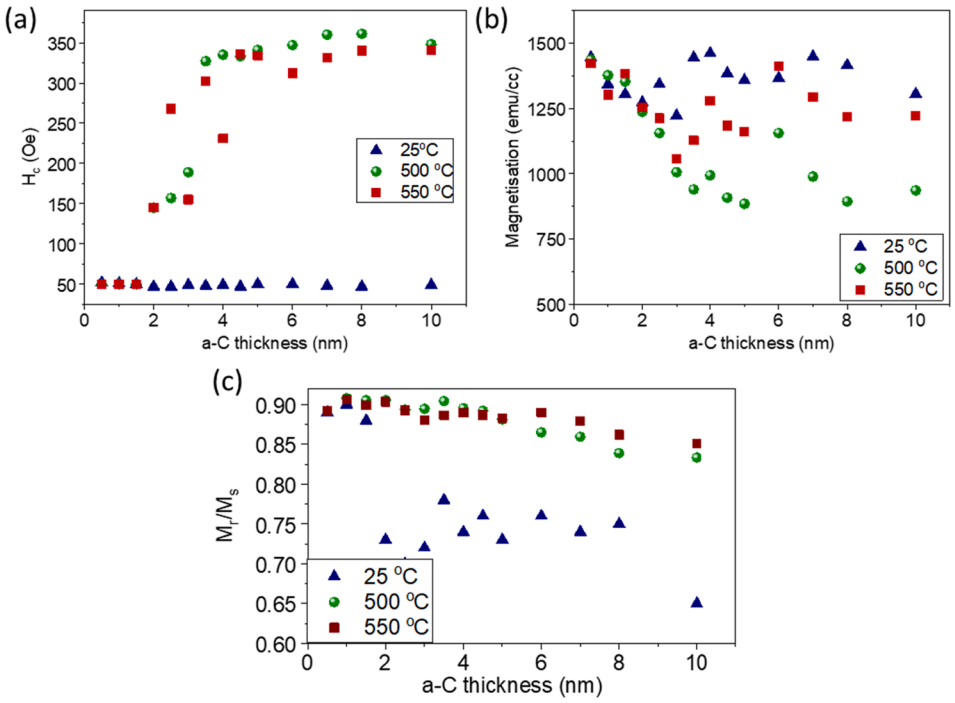

Fig. 4. Effect of annealing on the magnetic properties of Ta(3)/Fe(10)/a-C(t)/Fe(10)/Al(5) samples with t = 0.5–10 nm. All the data points presented are extracted from hysteresis loops at room temperature as-deposited or after annealing at 500 or 550 °C. (a) Coercivity H_c and (b) magnetization M_s. (c) Shows the remanence ratio of Ta(3 nm)/Fe(10 nm)/a-C(t)/Fe(10 nm)/Al(5 nm). M_r/M_s decreased with the increase of RF-sputtered a-C for all samples as- deposited and annealed at 500 °C and 550 °C.

indicated in Fig. 2a, b. This lower magnetization is likely due to metal/carbon interdiffusion at high temperatures, in particular when using Al cap layers. The formation of non-magnetic iron carbide layer at the Fe/a-C interfaces will also reduce the net magnetization of the system. [41,42]

Fig. 3 a and b show the change in H_c for these samples. H_c shows a reduction of a factor ~2 compared to as-deposited samples for annealing temperatures up to 300–400 °C. However, at 500–550 °C there is a

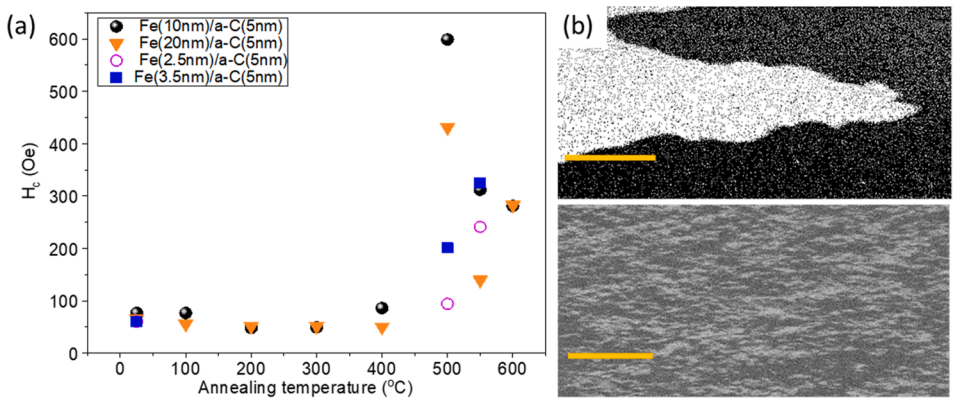

Fig. 5. The dependence of H_c on the annealing temperature for samples with different Fe thicknesses. Magneto-optic Kerr microscopy (MOKE) images taken at H_c show that an as- deposited sample of Ta(3 nm)/Fe(20 nm)/a-C(5 nm)/Al(5 nm) has large domains before anneal- ing (top right image) whereas annealing the same sample at 500 °C (H_c peak) for 10 h reduces greatly the domain size (bottom right image). Scale bars are 100 μm.

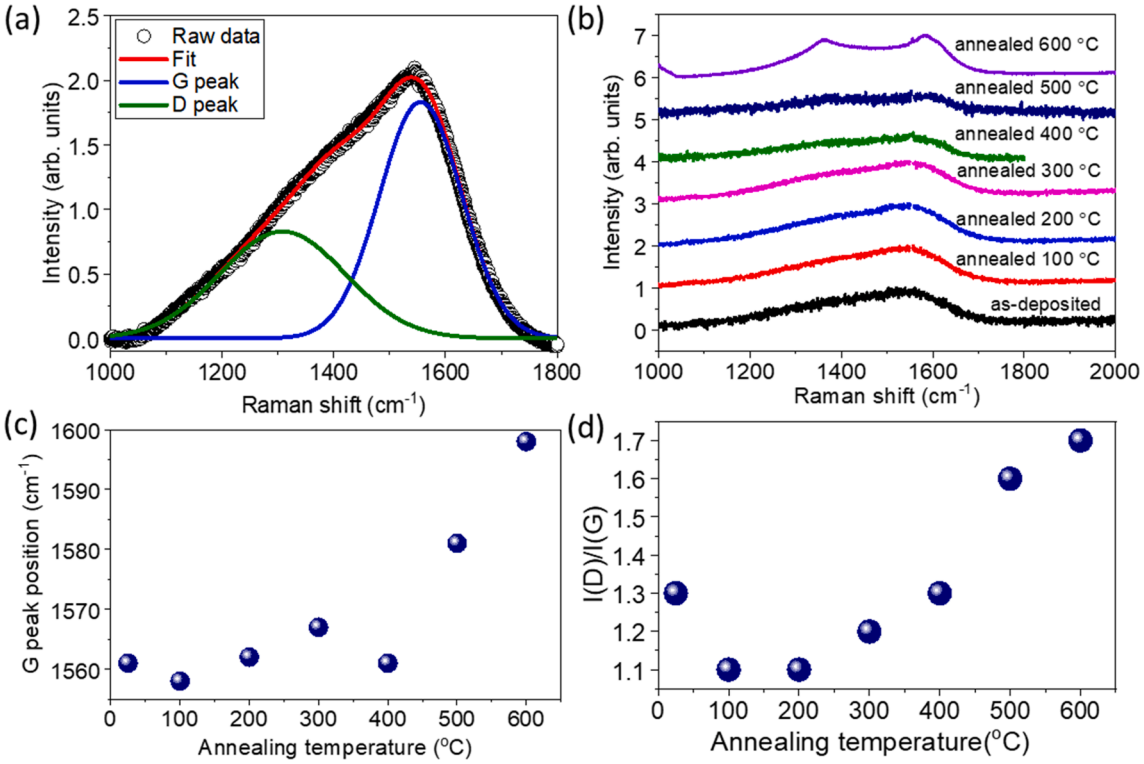

Fig. 6. Raman spectrum for a sample of Ta(3 nm)/Fe(10 nm)/a-C(5 nm)/Al(5 nm).(a) The (G and D) peaks as indicated by blue and green lines, respectively. (b) Raman spectrum of the a-C layers deposited on Fe films after annealing. (c) The position of the G peak (cm^{-1}) and (d). The intensity ratio I (D)/I (G) for samples at different annealing temperatures. The ratio change shows the sp^3 to sp^2 change in hybridisation.

tenfold increase in H_c from 60 Oe in as-deposited films to > 600 Oe. We attribute the change to carbon diffusion and changes in carbon structure from amorphous to nano-crystalline, leading to the formation of pinning points and small domains –see C. Structural Characterisation and magnetic images below. At higher temperatures, the pinning sites fuse with the iron film, reducing the magnetization further and leading to a drop in coercivity. [43] The interfacial effects in this metallo-carbon system lead to the possibility of making Fe/RF-sputtered a-C thin films with a controlled value of coercivity (H_c) between six times smaller and ten times larger than that of pristine iron.

As it happens for the bilayers, annealing trilayer Fe/a-C/Fe samples at temperatures < 400 °C lowers H_c, but increasing the annealing temperature to 500–550 °C also results in a larger (by a factor 7) coercivity. Notably, this increase only takes place when the a-C layer forms a continuous film, pointing to the importance of having a well-defined magneto-carbon interface layer in order to observe these effects. The hysteresis loop becomes also more square after annealing, resulting in higher remanence, see Fig. 4. The formation of domains after annealing leads the magnetization to align in a certain crystallographic direction that could enhance the magnetic anisotropy. The M_r/M_s ratio would then be affected by the magnetic anisotropy, [42] which is enhanced after annealing at 500 and 550 °C.

We use magneto-optic Kerr effect (MOKE) microscopy to study the magnetic domain configuration of Fe/a-C before and after annealing at 500 °C (see Fig. 5). The domains observed at the coercive field in Fe/a-C bilayers become much smaller and with lower contrast after annealing. The changes observed in the hysteresis loop and the MOKE images can be explained by a large increase in the density of pinning points. This can

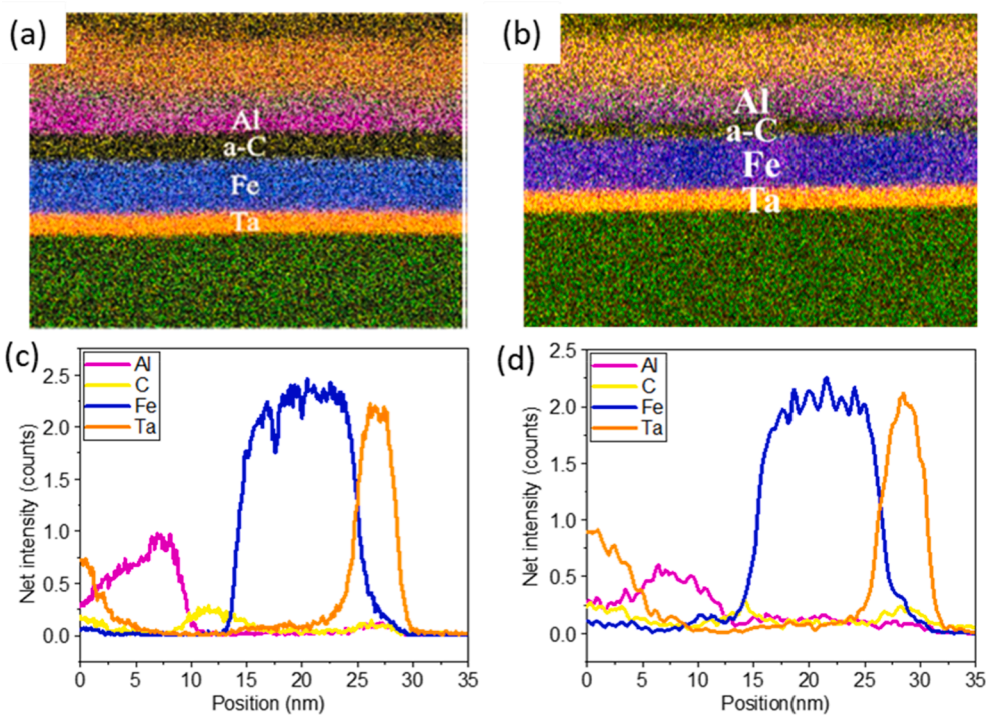

Fig. 7. Cross-sectional high resolution of Fe/a-C/Al films show that annealing may lead to carbon diffusion in iron. Image of Fe(10 nm)/RF-sputtered a-C(20 nm)/Al (5 nm) film (1) as-deposited and (b) annealed at 500 °C. Elementary line scans show the depth profile composition of the multilayers (c) before and (d) after annealing using TEM.

be expected as due to carbon atoms diffusing along grain boundaries of the iron thin film, although the crystallisation of the a-C layer may also play a role –see Raman measurements below. At temperatures above 500–600 °C, we form non-magnetic iron carbides. This carbon diffusion along grain boundaries, non-magnetic carbides and nanocrystalline carbon act as magnetic pinning points. The increased density of pinning points reduces the domain size (compare Fig. 5b and c), increasing the coercivity –see the discussion that follows.

2.3. Structural characterization

Next, we considered the change in morphology, diffusion and *sp* hybridisation of as-deposited and annealed a-C layers on Fe films. The vibrational modes for the different carbon allotropes are well known, and Raman spectroscopy is a straightforward technique to investigate these changes. The spectra after annealing show the D and G vibration modes at 1360 and 1600 cm^{-1}, as seen in Fig. 6a. The G band occurs due to the stretching of C-C sp^2 sites in both rings and chains, whereas the D band is due to the breathing of the sp^2present in rings only. [41]

A sample of Ta(3 nm)/Fe(10 nm)/a-C(5 nm)/Al(5 nm) was annealed at 100–600 °C for one hour in a vacuum 10^{-1} Torr. The Raman spectra of the Fe/RF-sputtered amorphous carbon with different annealing temperatures are presented in Fig. 6 b. The results show a shift in the G position from 1561 to 1598 cm^{-1} as presented in Fig. 6 c. At the same time, the I(D)/I(G) ratio increases from 1.3 to 1.7 after annealing, Fig. 6 d. These changes in the Raman spectrum are typical for the formation of nanocrystalline graphite and a change in the orbital hybridisation from (20%) $sp^2$to sp^2 only.[18,44,45]

Fig. 7 a and b show cross-section TEM images of a typical Ta(3 nm)/ Fe(10 nm)/ a-C(5 nm)/ Al(5 nm) structure before and after annealing to provide in-formation about atomic inter-diffusion. Fig. 7 c and d show the TEM elemental mapping across the layers before and after annealing. The as-deposited sample before annealing shows clear boundaries between the layers and smooth interfaces. [28,45] After annealing at 500 °C, the a-C layer has diffused partly into the iron layer, although it remains close to the surface. Furthermore, annealing leads to carbon diffusion along the Fe thin film grain boundaries. [46,47]

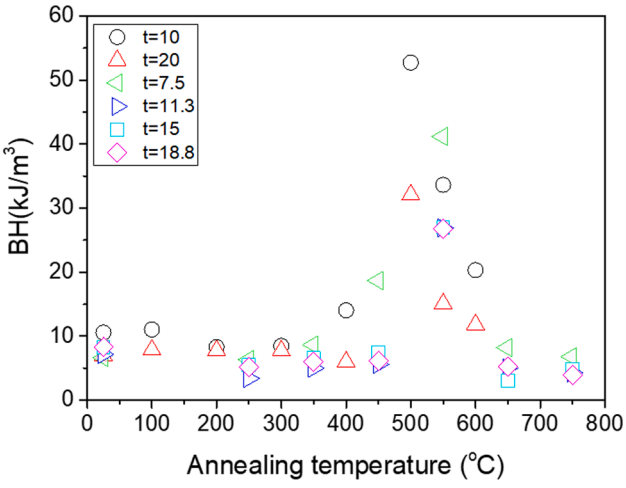

Fig. 8. Dependence of the maximum energy product on annealing temperature for Fe/RF- sputtered a-C with different Fe thicknesses. Note the peak at ~550 °C corresponding to the maximum coercivity and remanence that we attribute to the optimal anisotropy enhancement.

We can use the energy product $(BH)_{max}$ in order to monitor simultaneously changes to coercivity and magnetisation during annealing (see Fig. 8). Although thin films ideally do not generate stray fields and cannot be used in energy generation applications, hard magnets are of interest in spintronic and magnetic storage applications. Furthermore, the results could be extended to bulk samples fabricated by ball milling or other means. The magnetization after annealing at 500 °C remains high, whilst the coercive field increases, giving a maximum magnetic energy product for a-C/Fe bilayers of about 50–55 kJ/m^3. Whether this result can be reproduced in bulk form for permanent magnetism and

energy generation applications would be the object of future studies. Nevertheless, for computing and information storage applications, where a coercivity of the order of 500–1 kOe can be beneficial, the growth of annealing of an a-C layer may be a realistic path. Similarly, if a very soft, thin magnetic films are required, we have shown that as-deposited iron bilayers with a-C in between can have a coercivity as low as a few Oe.

3. Conclusion

The magnetic interfacial effects between iron and sputtered carbon were investigated in this work. The coercivity of iron films, typically of the order of 50–60 Oe, can be tuned by the deposition of a-C overlayers to be as low as 10 Oe in as-deposited films, and as high as 600 Oe after annealing, depending on the film thickness and post-growth processing. Raman spectroscopy and TEM analysis show that the a-C layer changes from amorphous carbon into nanocrystalline graphite and partly diffuses into the iron film upon annealing at 500–550 °C. This results in larger domain pinning, increasing the coercivity and reducing the domain size.

Our results show the effects of amorphous carbon layers grown via sputtering on the M_s and H_c of iron thin films. The softening and hardening of the hysteresis loop via hybridisation and atomic diffusion, with large effects of 500% in either direction, could open new paths to tailoring the interfacial magnetic anisotropy in ferromagnetic/nanocarbon systems. By heating locally regions of a Fe/a-C bilayer (e.g. via laser microscopy), we can also achieve local magnetic pinning and control the domain wall mobility and morphology. This has potential applications in e.g. the design of magnetic multilayers and for the use of amorphous carbon coatings in HAMR.

CRediT authorship contribution statement

Shoug Alghamdi: Investigation, Visualization, Writing – original draft. **Timothy Moorsom:** Methodology, Validation. **Fatma Al Ma'Mari:** Methodology, Validation. **Alistair Walton:** Investigation. **Zabeada Aslam:** Investigation, Visualization. **Mannan Ali:** Resources, Methodology. **Bryan J. Hickey:** Validation, Writing – review & editing. **Oscar Cespedes:** Conceptualization, Supervision, Writing – review & editing.

Declaration of Competing Interest

The authors declare that they have no known competing financial interests or personal relationships that could have appeared to influence the work reported in this paper.

Acknowledgments

We thank the UK Engineering and Physical Sciences Research Council (EPSRC) for support via grants EP/S030263/1, EP/M000923/1 and EP/K00512X/1. S.A. thanks Taibah University for support with a PhD scholarship.

References

[1] X. Liu, T. Miyao, A. Morisako, IEEE Trans. Magn. 42 (2006) 2772.
[2] M. Humphries (2013).
[3] N. Poudyal, J.P. Liu, J. Phys. D-Appl. Phys. 46 (2013).
[4] X. Crispin, V. Geskin, A. Crispin, J. Cornil, R. Lazzaroni, W.R. Salaneck, J.L. Bredas, J. Am. Chem. Soc. 124 (2002) 8131.
[5] M. Sagawa, S. Fujimura, N. Togawa, H. Yamamoto, Y. Matsuura, J. Appl. Phys. 55 (1984) 2083.
[6] C.B. Rong, V. Nandwana, N. Poudyal, J.P. Liu, M.E. Kozlov, R.H. Baughman, Y. Ding, Z.L. Wang, J. Appl. Phys. 102 (2007).
[7] D. Li, Y. Li, D.S. Pan, Z.D. Zhang, C.J. Choi, J. Magn. Magn. Mater. 469 (2019) 535.
[8] D. Babonneau, J. Briatico, F. Petroff, T. Cabioc'h, A. Naudon, J. Appl. Phys. 87 (2000) 3432.
[9] Y.H. Lee, T.C. Han, Jpn. J. Appl. Phys. Part 1-Regular Papers Brief Communications Review Papers 43 (2004) 7477.
[10] S.G. Yastrebov, V.I. Ivanov-Omskii, V. Pop, C. Morosanu, A. Slav, J. Voiron, Semiconductors 39 (2005) 840.
[11] E.P. Sajitha, V. Prasad, S.V. Subramanyam, S. Eto, K. Takai, T. Enoki, Carbon 42 (2004) 2815.
[12] T. Enz, M. Winterer, B. Stahl, S. Bhattacharya, G. Miehe, K. Foster, C. Fasel, H. Hahn, J. Appl. Phys. 99 (2006).
[13] T. Moorsom, M. Wheeler, T.M. Khan, F. Al Ma'Mari, C. Kinane, S. Langridge, D. Ciudad, A. Bedoya-Pinto, L. Hueso, G. Teobaldi, V.K. Lazarov, D. Gilks, G. Burnell, B.J. Hickey, O. Cespedes, Phys. Rev. B 90 (2014).
[14] K. Bairagi, A. Bellec, V. Repain, C. Chacon, Y. Girard, Y. Garreau, J. Lagoute, S. Rousset, R. Breitwieser, Y.C. Hu, Y.C. Chao, W.W. Pai, D. Li, A. Smogunov, C. Barreteau, Phys. Rev. Lett. 114 (2015).
[15] T.L.A. Tran, D. Cakir, P.K.J. Wong, A.B. Preobrajenski, G. Brocks, W.G. van der Wiel, M.P. de Jong, ACS Appl. Mater. Interfaces 5 (2013) 837.
[16] T. Moorsom, S. Alghamdi, S. Stansill, E. Poli, G. Teobaldi, M. Beg, H. Fangohr, M. Rogers, Z. Aslam, M. Ali, B.J. Hickey, O. Cespedes, Phys. Rev. B 101 (2020).
[17] F. Al Ma'Mari, T. Moorsom, G. Teobaldi, W. Deacon, T. Prokscha, H. Luetkens, S. Lee, G.E. Sterbinsky, D.A. Arena, D.A. MacLaren, M. Flokstra, M. Ali, M. C. Wheeler, G. Burnell, B.J. Hickey, O. Cespedes, Nature 524 (2015) 69.
[18] F. Al Ma'Mari, M. Rogers, S. Alghamdi, T. Moorsom, S. Lee, T. Prokscha, H. Luetkens, M. Valvidares, G. Teobaldi, M. Flokstra, R. Stewart, P. Gargiani, M. Ali, G. Burnell, B.J. Hickey, O. Cespedes, Proc. Nat. Acad. Sci. USA 114 (2017) 5583.
[19] F. Djeghloul, M. Gruber, E. Urbain, D. Xenioti, L. Joly, S. Boukari, J. Arabski, H. Bulou, F. Scheurer, F. Bertran, P. Le Fevre, A. Taleb-Ibrahimi, W. Wulfhekel, G. Garreau, S. Hajjar-Garreau, P. Wetzel, M. Alouani, E. Beaurepaire, M. Bowen, W. Weber, J. Phys. Chem. Lett. 7 (2016) 2310.
[20] O. Cespedes, M.S. Ferreira, S. Sanvito, M. Kociak, J.M.D. Coey, J. Phys.-Condens. Matter 16 (2004) L155.
[21] A. Ghasemi, S.E. Shirsath, X.X. Liu, A. Morisako, J. Appl. Phys. 111 (2012).
[22] M. Gruber, F. Ibrahim, S. Boukari, L. Joly, V. Da Costa, M. Studniarek, M. Peter, H. Isshiki, H. Jabbar, V. Davesne, J. Arabski, E. Otero, F. Choueikani, K. Chen, P. Ohressee, W. Wulfhekel, F. Scheurer, E. Beaurepaire, M. Alouani, W. Weber, M. Bowen, Nano Lett. 15 (2015) 7921.
[23] S. Boukari, H. Jabbar, F. Schleicher, M. Gruber, G. Avedissian, J. Arabski, V. Da Costa, G. Schmerber, P. Rengasamy, B. Vileno, W. Weber, M. Bowen, E. Beaurepaire, Nano Lett. 18 (2018) 4659.
[24] M. Gruber, F. Ibrahim, S. Boukari, H. Isshiki, L. Joly, M. Peter, M. Studniarek, V. Da Costa, H. Jabbar, V. Davesne, U. Halisdemir, J.J. Chen, J. Arabski, E. Otero, F. Choueikani, K. Chen, P. Ohresser, W. Wulfhekel, F. Scheurer, W. Weber, M. Alouani, E. Beaurepaire, M. Bowen, Nat. Mater. 14 (2015) 981.
[25] J. Matlak, K. Komvopoulos, Sci. Rep. 8 (2018).
[26] C. Casiraghi, J. Robertson, A.C. Ferrari, Mater. Today 10 (2007) 44.
[27] J. McLaughlin, P.M.A. Ogwu, R. Lamberton, J.F. Zhao, P. Lemoine, Int. J. Mod. Phys. B 14 (2000) 167.
[28] S.H. Vijapur, D. Wang, G.G. Botte, Carbon 54 (2013) 22.
[29] F.J. Derbyshire, A.E.B. Presland, D.L. Trimm, Carbon 13 (1975) 111.
[30] K. Oohashi, T. Hirose, T. Shimamoto, J. Struct. Geol. 33 (2011) 1122.
[31] T.J. Konno, R. Sinclair, Acta Metall. Mater. 43 (1995) 471.
[32] A.G. Ramirez, T. Itoh, R. Sinclair, J. Appl. Phys. 85 (1999) 1508.
[33] S. Tajima, S. Hirano, J. Mater. Sci. 28 (1993) 2715.
[34] A.B. Wu, D.M. Liu, L.Z. Tong, L.X. Yu, H. Yang, CrystEngComm 13 (2011) 876.
[35] R. Sinclair, T. Itoh, R. Chin, Microsc. Microanal. 8 (2002) 288.
[36] R.A. Rodriguez, A.N. Conejo, Issss, Issss, and Issss, in: *60th Ironmaking Conference Proceedings*; *vol. 60,* 2001, p. 669.
[37] J. von Appen, B. Eck, R. Dronskowski, J. Comput. Chem. 31 (2010) 2620.
[38] D.A. Mirzayev, A.A. Mirzoev, I.V. Buldashev, K.Y. Okishev, Phys. Met. Metall. 119 (2018) 1148.
[39] R. Krishnan, H.O. Gupta, C. Sella, M. Kaabouchi, J. Magn. Magn. Mater. 93 (1991) 174.
[40] A.K. Shokanov, M.F. Vereshchak, I.A. Manakova, A.N. Ozernoy, Z.K. Tleubergenov, K.A. Bedelbekova, V.I. Yaskevich, Crystallogr. Rep. 65 (2020) 363.
[41] A.C. Ferrari, J. Robertson, Phys. Rev. B 64 (2001).
[42] A.C. Ferrari, J. Robertson, Philos. Trans. Roy. Soc. A – Math. Phys. Eng. Sci. 362 (2004) 2477.
[43] A. Javed, N.A. Morley, M.R.J. Gibbs, Appl. Surf. Sci. 257 (2011) 5586.
[44] A.C. Ferrari, J. Robertson, Phys. Rev. B 61 (2000) 14095.
[45] J. Robertson, Mater. Sci. Eng. R-Reports 37 (2002) 129.
[46] C. Coutts, M. Arora, R. Hubner, B. Heinrich, E. Girt, AIP Adv. 8 (2018).
[47] G.L. Katona, I.A. Vladymyrskyi, I.M. Makogon, S.I. Sidorenko, F. Kristaly, L. Daroczi, A. Csik, A. Liebig, G. Beddies, M. Albrecht, D.L. Beke, Appl. Phys. A-Mater. Sci. Process. 115 (2014) 203.